The "Why" and "How" of JointICA: Results from a Visual Detection Task

Bogdan Mijović[a,b], Maarten De Vos[a,b,c], Katrien Vanderperren[a,b], Nikolay Novitskiy[d], Bart Vanrumste[a,e], Peter Stiers[f], Bea Van den Bergh[d,g], Johan Wagemans[d], Lieven Lagae[h], Stefan Sunaert[i], Sabine Van Huffel[a,b]

[a]*Katholieke Universiteit Leuven, Department of Electrical Engineering, ESAT-SCD, Leuven, Belgium*

[b]*IBBT-K.U.Leuven Future Health Department, Leuven, Belgium*

[c]*Oldenburg University, Department of Psychology, Neuropsychology Lab, Oldenburg, Germany*

[d]*Katholieke Universiteit Leuven, Department of Psychology, Laboratory of Experimental Psychology, Leuven, Belgium*

[e]*Katholieke Hogeschool Kempen, Biosciences and Technology Department, Geel, Belgium*

[f]*Maastricht University, Faculty of Psychology and Neuroscience, Maastricht, The Netherlands*

[g]*Tilburg University, Department of Psychology, Tilburg, The Netherlands*

[h]*Katholieke Universiteit Leuven, Department of Pediatric Neurology, Leuven, Belgium*

[i]*Katholieke Universiteit Leuven, Department of Radiology, Leuven, Belgium*

Abstract

The multimodal analysis of brain activity is becoming more and more popular among the research community. One of these concerns the integration of simultaneously acquired electroencephalographic (EEG) and functional magnetic resonance imaging (fMRI) data. However, no standard approach has been established so far. One of the possible data-driven methods consists in the joint analysis of event related potentials (ERPs) and fMRI maps derived from the response to a particular stimulus. Such an algorithm (joint independent component analysis or JointICA) has recently been proposed by Calhoun et al. (2006). The algorithm has shown to perform well, and to

provide meaningful results. However, the algorithm's performance has not been fully characterized yet, and no procedure has been proposed to assess the quality of the decomposition. In this paper we therefore try to answer why and how JointICA works. We show the performance of the algorithm on data obtained in a visual detection task, and compare the performance for EEG recorded simultaneously with fMRI data and for EEG recorded in a separate session (outside the scanner room). We perform several analyses in order to characterize the performance of the algorithm in more detail, to set the necessary conditions which will lead to a sound decomposition, and to make it more transparent to potential future users.

Introduction

The activation of a particular brain area consists in the synchronized firing of a subpopulation of neurons in that area, involved in processing information or executing a particular task. The synchronized relevant neural firing can be measured with the electroencephalogram (EEG) as event-related potentials (ERP). Back in 1889, Roy and Sherrington (1889) suggested that neural activity is accompanied by a regional increase in cerebral blood flow. Since 1991, these regional cerebral blood flow changes can be measured directly as the Blood Oxygenation Level Dependent (BOLD) signal with functional Magnetic Resonance Imaging (fMRI).

Moreover, EEG and BOLD changes can be measured simultaneously to benefit from their complementary properties. EEG measures electrical responses with a millisecond precision, but does not provide a precise spatial localization of the underlying cortical activity, since the electrode position is limited to the scalp surface. fMRI, on the other hand, measures local changes in brain hemodynamics with a very good spatial precision. However, the hemodynamic response is a slow signal and one Echo-Planar Image (EPI) is only acquired every few seconds. This is far below the brain reaction time

to externally applied stimuli, thus making the analysis of detailed temporal brain changes during the reaction on external stimuli very difficult.

For this reason, the simultaneous acquisition of both EEG and fMRI is getting more and more popular, as their complementarity can provide deeper insight into function and dysfunction of brain dynamics (Ullsperger and Debener, 2010; Mulert and Lemieux, 2010; Debener and De Vos, 2010). This advantage has already been exploited in numerous applications. For instance, the combination of EEG and fMRI allows localizing epileptic activity based on spike-triggered fMRI (Seeck et al., 1998; Krakow et al., 2001; Lemieux et al., 2001; Bénar, et al., 2006). Other possible applications are the study of ongoing brain rhythms (Goldman et al., 2000 2002; Laufs et al., 2003; Moosmann et al., 2003) and cerebral activations during sleep (Czisch et al., 2002; Liebenthal et al., 2003; Schaubs et al., 2007). Also the analysis of event-related brain responses based on multimodal information (Mulert et al., 2004; Debener et al., 2005, 2006; Calhoun et al., 2006; Eichele et al., 2008; Moosmann et al., 2008) becomes more and more popular.

In recent years, several integration approaches have also been proposed. The earliest proposed methods were EEG-informed fMRI and fMRI-informed EEG analysis. These approaches are asymmetric, meaning that one of the modalities is considered to be prior knowledge to improve the results in the other modality. In fMRI-informed EEG, the fMRI sources are used to improve the localization of the ERP generators. In EEG-informed fMRI the ERP information is used to model the strength of the hemodynamic response based on single-trial ERP amplitude modulations, with the aim of localizing the modulation-related fMRI sources.

Data-driven signal processing techniques are well-established for processing EEG

data (e.g. De Vos et al., 2007, 2010; Viola et al., 2009), and are getting more and more popular for analyzing fMRI data (in the temporal domain: McKeown et al., 1998a, 1998b; McKeown, 2000; and in the spatial domain: Calhoun et al., 2001, 2004). They are also increasingly used for exploiting advantages of combined EEG-fMRI measurements. Attractive methods for this purpose are blind source separation (BSS) algorithms, such as independent component analysis (ICA), and canonical correlation analysis (CCA) (Ullsperger and Debener, 2010). The best-known ICA-based algorithms for integrated EEG-fMRI analysis are Parallel ICA (Eichele et al., 2008; Calhoun et al., 2009), and JointICA (Calhoun et al., 2006, 2009), which will now be explained in more detail. CCA-based methods are not the focus of this paper; we refer the reader to Corea et al. (2008, 2010) for more information.

The Parallel ICA algorithm identifies components in both modalities separately, applying spatial ICA to fMRI data, and temporal ICA to single trial EEG data (Eichele et al., 2008). After extracting the independent components from both modalities, the corresponding components are identified based on correlations between trial-to-trial fluctuations in the temporal domain. Although the Parallel ICA algorithm shows a nice performance in data-fusion applications, it is not entirely multimodal, since the data have been processed separately, and connections are only identified afterwards.

JointICA, on the other hand, identifies the independent components of both modalities simultaneously. To do this, it starts from ERP epochs in the temporal domain and fMRI activation maps in the spatial domain. In the original paper on JointICA (Calhoun et al., 2006), the method was applied to averaged ERP data from different participants. Although another possible application has been shown on single-trial simulation data by Moosmann et al. (2008), in this paper we will focus on the original

algorithm on averaged data. The method assumes that the different components (peaks) of the ERP and the hemodynamic response corresponding to the same stimulus are generated in the same brain region (as proposed by Logothetis et al., 2001), and that they are therefore statistically dependent. Hence, it is believed that ICA will be able to disentangle these components and connect the electrical activations (ERP peaks) to their corresponding chemical (BOLD) brain activations (Calhoun et al., 2006).

The hypothesis about this one-to-one relation between physiological origin and statistical dependence, however, is not necessarily true, since there is no particular mathematical reason to ensure capturing different ERP peaks always together with their corresponding fMRI activations. First of all, spatial statistical independence among fMRI components alone cannot be justified in the sense that there is no physical reason for the spatial samples to correspond to different activity patterns with independent distributions (see Daubechies et al. 2009). Moreover, the probability density function of spatial fMRI component maps has a Gaussian distribution, which by definition cannot be decomposed using common ICA algorithms. Furthermore, the two signals (ERP and fMRI) are very different in nature from a signal processing point of view. ERP is a temporal signal and fMRI a spatial map without any temporal information and their distributions are undoubtedly different. Therefore, it seems difficult to capture them in a single component, if this component has to be generated solely based on the statistical properties of the signals.

Although JointICA was shown to work well when introduced as a tool for integrated ERP and fMRI data analysis (Calhoun et al., 2006, 2009) and to give meaningful results with real data, the abovementioned underlying assumption was not questioned. Accordingly, and because of a growing interest in the method (Calhoun et al.,

2010; Franco et al., 2008; Xu et al., 2009), some more methodological concerns need to be investigated.

In this paper we therefore try to explore and validate the performance of JointICA and its central assumption that physiological linking between ERP and BOLD amplitudes drives the extraction of multimodal components despite their intrinsically different temporal and spatial nature. We also show that the ICA algorithm used in the JointICA method (Infomax - Bell and Sejnowski, 1995) plays a crucial role in this multimodal separation. To support this claim, we investigate the performance of JointICA when another well-known ICA algorithm is used (JADE – Cardoso and Souloumiac, 1993), and show that this does not allow dealing with these fused data.

To validate the meaningfulness of the JointICA results, we used a well-established simple visual detection task with known ERP components and fMRI activation sites [Reference to Di Russo], thus well-suited for validation purposes. The contribution of the central linking hypothesis was evaluated first by randomly reassigning ERPs and fMRI activation maps over participants, thus destroying the amplitude link between the two modalities, and second by a comparison with an individual ICA analysis of both ERPs and fMRI maps, thus excluding any intermodal interaction. Furthermore, we investigated the effect of the ERP quality for JointICA by comparing recordings inside and outside of the scanner and the dependence of the JointICA results on the sample size.

Based on the results obtained with these different analyses we will discuss why and when (under which conditions) JointICA works well, hopefully providing a better understanding for potential future users.

Materials and methods

Subjects

Fifteen healthy subjects (4 female and 11 male, aged 21-33) with no history of neurological or cardiological disorders participated in this study. Written informed consent was obtained in accordance with the local ethical committee guidelines. During the simultaneous measurements subjects were lying supine in the scanner on a cushion that ameliorated the pressure from the EEG electrodes on the head, and with soft cushions to the side to restrict head movement in the coil. Subjects were provided with earplugs and headphones to avoid any harmful effect from the fMRI acoustic noise. Nine out of these fifteen subjects additionally participated in a session where only EEG was acquired outside of the scanner room with the same presentation paradigm.

Tasks

Participants performed a simple visual detection task while in the scanner. Stimuli consisted of segments of circular black-and-white checkerboard stimuli presented one at a time in randomized sequences to one of the four quadrants of the visual field (Di Russo et al., 2003, 2005). A central stimulus was also present, but was not used for the purpose of this study. Subjects were asked to press a button upon detection of each of these stimuli. Per run 100 stimuli (20 of each type) were shown to the participants. The Inter-Stimulus Interval (ISI) varied between 900 ms and 1900 ms. A more detailed description of the task can be found in Novitskiy et al. (2011).

Data acquisition

All subjects performed 4 runs of the visual detection task. For validation purposes the EEG data were not only acquired in the magnetic field of the scanner, but 9 out of 15 subjects also performed the same task outside the scanner room. The EEG data were collected from 62 standard scalp sites using the BrainAmp MR+ system (BrainProducts, Munich, Germany) with a sampling rate of 5 kHz. All channels were recorded with FCz as reference and Iz as ground. Electrode impedances were kept below 10 kΩ. fMRI data were recorded with a Philips 3T Intera whole-body scanner. During each experimental block, 160 echo-planar images (EPI) composed of 28 slices of 3 x 3 x 4.5 mm voxel size and 4.8 mm slice thickness were recorded with ascending slice order and 1.95 second repetition time (TR). For anatomical reference, full brain anatomical images were obtained with the magnetization prepared rapid gradient echo (MPRAGE) imaging sequence (230 coronal slices, time to echo [TE] = 4.6 ms, TR = 9.7 s).

EEG processing

Preprocessing of the acquired EEG data was performed in the MATLAB 7.7.0 (R2008B) (The Mathworks Inc, Natick, Massachusetts, USA) environment with the EEGLAB 5.03 toolbox (Delorme and Makeig, 2004).

First, *gradient* artifacts were removed with the average template subtraction method (Allen et al., 2000), as implemented in the Bergen EEG-fMRI EEGLAB plug-in (Moosmann et al., 2009). After filtering and downsampling to 500Hz, *ballistocardiogram*

(BCG) artifact removal was performed with the Optimal Basis Set (OBS) method (Niazy et al., 2005) by creating an artifact template with 3 principal components (as validated in Vanderperren et al., 2010). Then, data were segmented from 100 ms before until 800 ms after stimulus onset, artifact-rejected at 200 μV, baseline corrected (-100 – 0 ms) and re-referenced to the average of TP9 and TP10 (the closest electrodes to the mastoids in the present electrode setup). Thereafter, an average ERP for each stimulus type was computed, and these averaged ERPs were further fed into the JointICA analysis (see below). The EEG data recorded outside the scanner were only filtered and downsampled and averaged ERPs were created in the same way as explained above.

For the application of the JointICA algorithm, only the ERP data from the electrodes PO7 and PO8 were used to observe the activations corresponding to right and left visual fields respectively. Only the ERPs from one of the electrodes are used for one analysis.

fMRI processing

fMRI analysis was performed with the statistical parametric mapping software (SPM5, Wellcome Department of Cognitive Neurology, London, UK) in MATLAB. The EPI time series were slice-time corrected, realigned, co-registered with anatomical images, normalized to a template and smoothed with an 8-mm FWHM Gaussian kernel.
A stick function at the onset of the stimulus as in traditional event-related fMRI studies was used as regressor. First-order statistics were calculated by convoluting the stick function at the stimulus timing with a canonical hemodynamic response function (HRF), separately for the 4 stimulus locations (upper-left – UL, upper-right – UR, lower-left –

LL, and lower-right – LR). No derivatives were used in the analysis. The 6 movement parameters (three for both translation and rotation) obtained during realignment were inserted in the model as covariates of no interest. As a result, the design consisted of 4 + 6 = 10 variables per experimental block per subject.

JointICA

JointICA has originally been proposed by Calhoun et al. (2006). The JointICA algorithm assumes that the electrical correlate of brain activation (expressed in the ERP components) and the hemodynamic response to brain activation (BOLD response) are generated by the same population of neurons. Hence, the amplitudes of the ERP wave (peak) and of the BOLD response invoked by an activated area will increase and decrease simultaneously: a stronger ERP peak activation will yield a stronger BOLD response in this particular brain region, and vice versa

Following this assumption, we can concatenate the SPM-derived fMRI activation map, derived from contrasting the BOLD signal invoked by a particular stimulus with the background, with the average ERP response corresponding to the same stimulus. Since the number of voxels in the fMRI map and the number of time samples in the ERP signal largely differ (the number of voxels is of the order of hundreds of thousands, whereas the number of ERP time points is usually around 1000), the resampling of one of the modalities is necessary for the ICA step. Otherwise, the analysis would be biased and give much more importance to fMRI compared to ERP data. Since downsampling the fMRI data by a factor 100 would lead to great loss of data, the ERP data are upsampled

by an integer (using cubic spline interpolation), to obtain a similar number of samples in the ERP as the number of voxels in the fMRI.

After upsampling, the data of the two modalities are normalized (transformed to z-scores, by subtracting the mean and dividing by its standard deviation) and concatenated into a single vector for each subject. The data from all the *m* subjects are then stacked into an *m* by *n* matrix (*m* being the number of subjects, *n* the number of samples of our artificially created data), and finally fed into an ICA algorithm to solve the linear mixing problem given in equation (1).

$$[\mathbf{X}^{fMRI} \quad \mathbf{X}^{EEG}] = \mathbf{A} \times [\mathbf{s}^{fMRI} \quad \mathbf{s}^{EEG}] \qquad (1)$$

X and **s** represent the mixture and the source matrices of the two modalities respectively, each consisting of an fMRI and EEG matrix part (annotated by superscripts *EEG* and *fMRI* in equation (1), corresponding to the modalities). Equation (1) assumes the same mixing matrix **A** for both modalities. As mentioned before, this means that the ERP peaks and the BOLD responses of the corresponding brain regions are assumed to be changing with the same dynamics.

Following what has been mentioned above, the JointICA algorithm provides, as an output, independent components, each containing the sources of both modalities (EEG and fMRI). In the results section, these components are always shown in paired figures, one containing EEG, and the other one fMRI information.

The ICA algorithm used in this setup is the Information Maximization algorithm (Infomax), proposed by Bell and Sejnowski, (1995). The number of independent

components to be estimated in our work was always set to 12, as in the original work of Calhoun et al., (2006).

ERP-fMRI Movie

The JointICA algorithm yields independent components as output. Each component consists of an ERP- and an fMRI-related part. We can regard these components as temporal (ERP) information of the spatial (fMRI) components. Having this output, it is possible to make an ERP-fMRI movie, which allows observing how the spatial maps change over the time of the ERP complex. Each time slice of the movie is computed in the following way:

$$fMRI_{movie}(t) = \sum_{i \subset IC}(ERP_i(t) \cdot fMRI_i) \qquad (2)$$

In equation (2), i belongs to a subset of chosen ICs, $fMRI_{movie}(t)$ represents one ERP-fMRI movie time slice at time t, ERP_i is the amplitude of the i-th ERP-related IC at time t, and $fMRI_i$ is the spatial functional map of the i-th IC, which, alone, contains no temporal information whatsoever. The $fMRI_{movie}$ from equation (2) can be considered as a sum of fMRI component maps weighted by the strength of the corresponding ERP components at a given time point.

Application of ICA and JointICA

To investigate the performance of JointICA, we start with applying it to the ERP and fMRI data recorded simultaneously. We visually validate the technique by checking the localization of the beginning of the fMRI response, which is time-related to the P1 component of the ERP. It has to be noted here that visual detection should normally activate first the primary visual area, which would be reflected in the C1 peak of the ERP (Di Russo et al., 2003, 2005). However, since this peak is not visible on PO7 and PO8 electrodes, we expect as a first correlate of visual processing the P1-related fMRI activation in extrastriate visual areas on the contra-lateral side of the brain (as shown in Di Russo et al. 2003, 2005). We check this for all 4 stimulus types.

Since only the averaged ERP is used in this study, the information embedded in the ERP should theoretically not differ between the EEG recorded simultaneously with fMRI, and the EEG acquired separately in another (outside) session. To check whether the quality of separation with ICA can be improved, we additionally performed the same analysis, but this time with the ERP data recorded outside the scanner room before or after the fMRI acquisition, and compared the results with the results from the first study. ERPs measured outside the scanner room should have a higher signal-to-noise-ratio than the ones recorded simultaneously due to the absence of scanner-related artifacts.

In order to quantify the similarity between components retrieved with these two analyses, we computed the correlation between their corresponding components. These correlations were determined in the temporal domain for the ERP aspect of the component and in the spatial domain for the fMRI component parts. The corresponding

component from the inside measurement is determined as the component which has the highest correlation coefficient with the one from the outside measurements.

As explained before (see equation (1)), JointICA assumes that the strength of both EEG and fMRI responses has the same pattern over subjects. To verify this hypothesis, we connected random ERP and fMRI data (corresponding to different subjects) and applied the algorithm to check how the decomposition is affected. In this case, the amplitudes of ERP and fMRI responses will not change simultaneously, since they come from different subjects.

In addition, we also applied the Infomax algorithm separately to ERP and fMRI data to show the difference for both modalities compared to the JointICA analysis on the simultaneously acquired data. Based on these analyses we expect to understand whether the JointICA algorithm separates components and sources based on the interaction between both modalities, or whether the separation of one of the modalities is influenced (or driven) by the separation of the other one.

Another important aspect to check is whether the choice of the ICA algorithm influences the goodness of the separation. We will therefore compare the performance of Infomax ICA to another well-known ICA algorithm (JADE) (Cardoso and Souloumiac, 1993).

Finally, we investigate the robustness of the method by leaving out several subjects and checking whether the decomposition is affected. We performed this analysis for 10, 11, 12 and 13 subjects, and compared the results to the original 15 subjects.

The number of extracted independent components was 12 in each of the abovementioned studies. We were limited to less than 15 components due to the number of subjects, but this number is also in accordance with the original work of Calhoun et al.

(2006). However, whilst the number of components remained 12 for 12 and 13 subjects in the robustness analysis, it dropped to 10 for 10 and 11 subjects.

For all the additional studies we will present and discuss the results only for the stimulus appearing in the down-left visual field, but the conclusions for other stimuli are similar.

Moreover, to make our conclusions more apparent, we defined three different categories of extracted independent components, according to the following criterion: category 1 consists of independent components, whose ERP modality energy is mostly situated in the stimulus-response time window between 50 and 400 ms after stimulus onset (more than 80% of the total energy of the component is in this interval). The second group comprises components that still contain more than 0.01% of the total ERP signal energy, but their main activity is not in the abovementioned time window (they mostly have late activations). The third category includes components whose energy does not influence the ERP signal, i.e. the ERP part of the independent component is a flat line (less than 0.01% of the total ERP energy).

Results

Simultaneous Measurements

In this section we present the results of the analyses on our simultaneous measurements in two ways. In Fig. 1, the JointICA decomposition is shown for the down-left visual field stimulus. In Fig. 2, we present the results of the first brain activations that

appear from the ERP-fMRI movie construction. These activations are presented for all four quadrant stimuli, overlaid in different colors.

Fig. 1 shows the results of applying the JointICA algorithm to the down-left stimulus data. The grand average ERP, together with the IC ERP wave, is shown on the right side, whereas the left side of the picture presents the corresponding fMRI activations related to these ERP IC peaks. Only the positive fMRI activations are shown. We focus here on category 1 components mostly. The locations of the fMRI activations in the brain are given in MNI coordinates. The fMRI occipital activations, which are connected to P1 and N1 ERP peak components (top row – Comp 003), appear most pronounced on the contra-lateral side compared to the stimulus. They activate visual areas, particularly the supracalcarine cortex (area V1/V2), and the left middle occipital gyrus (Lateral Occipital Complex – LOC area), which have been associated with P1 activation. Less extensive mirror activations are seen on the ipsi-lateral side. These activations are expected, and are in line with previous findings in literature (Martinez et al., 2001; DiRusso et al., 2003, 2005; Calhoun et al., 2006)

However, it is apparent that the decomposition of the ERP wave for this component is not perfect. For instance, the component containing the P2 peak does not follow the double hump present in the data (see middle row, Comp 007). Also, the activations corresponding to both P1 and N1 peaks are combined into one independent component. Additionally, this component only shows weak fMRI activation of the motor cortex area, whereas we do expect the motor activation to be connected to the N1 peak (Calhoun et al., 2006). On the other hand, the bottom component in Fig. 1 (Comp 001) corresponds to clear somatosensory motor activity, but has no ERP response (i.e., a category 3 component, which is given here as an example).

To further investigate which regions are active at a certain time instant, independent components can be back-projected and combined in an ERP-fMRI movie, and the fMRI spatio-temporal map can be obtained, as explained in the Methods section. In Fig. 2 we show the first fMRI activations that emerge in the fMRI spatio-temporal map, which can be considered the beginning of the visual activation. These activations for down-left (DL), down-right (DR), upper-left (UL) and upper-right (UR) stimuli are presented in different colors. The corresponding ERPs with their JointICA decomposition are shown in the corners, in colors describing the corresponding stimulus. This figure is different from Fig. 1, in the sense that it shows a recombination of the spatial maps of several independent components weighted by the strength of their associated ERP signal at a certain time instant (like described previously in the *ERP-fMRI Movie* section), whereas each row in Fig. 1 shows only one independent component with its fMRI map and its ERP time-course in two different plots.

From Fig. 2, it is obvious that activation starts in the contra-lateral hemisphere of the brain, as expected. The fMRI maps associated with the down-left stimulus (shown in yellow) include all the expected activations described in literature, namely early visual areas, lateral occipital, and ventral stream activation. The primary visual cortex activations are detected for both of the left sided stimuli on opposite sides of the calcarine sulcus, as expected.

On the other hand, for the stimuli presented on the right side no primary visual activity was recovered. It is interesting to note here that V1/V2 fMRI activity is known to correspond to the C1 peak in the ERP, which cannot be captured with the PO7 and PO8 electrodes used in this study (Martinez et al., 2001; Di Russo et al., 2003). However, the activity is still present in the fMRI modality and has to be present in one of the

components. Therefore, it may be expected that this activation is sometimes successfully associated with the first fMRI activation, but it is also possible that sometimes it is missing.

The activation in the ventral occipital cortex is visible only for down-left and upper-right stimuli, whereas it is missing for down-right and upper-left stimuli. This means that the JointICA algorithm applied to simultaneously recorded EEG and fMRI data captures meaningful composite brain activity, although the decomposition itself can still be improved.

Non - Simultaneous Measurements

In addition to the simultaneous acquisition, a non-simultaneous EEG measurement was performed, where the data was recorded during the same task performed outside of the scanner room. This second measurement was free of the magnetic field artifacts that distort the simultaneously acquired EEG.

Fig. 3 shows the results of applying the JointICA algorithm to the fMRI data from the simultaneous measurement combined with the ERPs derived from the non-simultaneous measurement, again for the down-left stimulus condition. Only three out of 12 extracted components are shown; again those of which the EEG independent components are closely related to the ERP activations (peaks) of the original signal – category 1.

The left side of the figure presents the corresponding fMRI components related to these peaks in blue. For the sake of comparison, the fMRI results for the corresponding fMRI activations from the simultaneous measurements (from Fig. 1) are overlaid in red,

and the overlap between the two is shown in magenta. Only positive fMRI activations are shown. The grand average ERP (in red) and the independent ERP components (in green, blue and magenta) are shown on the right.

It is obvious that the fMRI activations for the inside and outside measurements largely overlap. As it was the case for the inside recorded EEG, contra-lateral fMRI activation is visible in the supracalcarine cortex (V1/V2 area), and the middle occipital gyrus (LOC area). However, differences are also apparent. The component containing the N1 ERP wave, for instance, is now associated with activation in the left post-central gyrus, corresponding to the primary somato-sensory cortex. This activation of motor-related activity, which is expected from previous studies, was not present in the simultaneously recorded data, and shows that the decomposition is improved when ERP data is recorded in a separate session.

Moreover, from this figure it can be seen that the P1 component is now not only connected to the N1, as was the case in the inside measurements, but it is also visible in the component showing the P2 peak. This decomposition is in line with the findings of Di Russo et al. (2003), where it was shown that the activities of the P1 generators will continue during N1 and P2 peaks. Additionally, the ERP component corresponding to P2 now closely follows the shape of the grand average P2 peak. This is contrary to our observations with simultaneously recorded EEG data.

The bottom row of Fig. 3 shows an ERP component with fMRI activations that are hard to interpret. By closer inspection of the back-reconstructed ERP part of this component over subjects, we noticed it to explain inter-subject N1 latency differences.

Fig. 4 shows the combined, back-projected independent components, similar to Fig. 2, but obtained with non-simultaneously recorded EEG. Again, the weighted

activation maps at the first ERP peak are shown, separately for down-left, down-right, upper-left and upper-right stimuli. It is obvious that the fMRI activations connected to the P1 ERP component again start in the primary visual cortex, contra-lateral to the stimulated visual quadrant, illustrating the robustness and correctness of the decomposition.

The activations corresponding to the left stimuli again show the double opponency regarding the stimulated visual field quadrant, and all the expected activations as described in the previous section (primary, lateral and ventral occipital) are detected. However, the upper left stimulus condition additionally shows more right parietal activity.

Concerning the right visual field stimulations, the outside ERPs improve the detection of the primary response for the upper right activation, yielding left inferior calcarine activity. However, the primary response in the down-right stimulus still remained undetected. Whilst both the upper and lower right stimuli are associated with ventral occipital activity, only the down-right stimuli were associated with activations of the lateral occipital cortex. This condition additionally showed activity in the left parietal area and in the motor cortex.

To conclude, these results confirm that the decomposition of the fMRI maps is improved when outside EEG data are used, instead of simultaneously recorded EEG.

To further verify the decomposition of the outside measurements, in Fig. 5 we show the activations in different time instants and we compare these results to the ones obtained by Martinez et al. (2001) and Di Russo et al. (2003), where the same down-left stimulus was used. In this figure, we show the fMRI activations from the spatio-temporal fMRI maps derived by the ERP-fMRI movie, at three different time instances,

corresponding to three different ERP peaks, namely C1, P1 and N1. The contra-lateral activations are marked with circles and their mirror ipsi-lateral activations are marked with squares. The new time-slice is presented only when the new activation appears for the first time, whereas the previous activations may still be present on the map.

It is apparent that activation in the calcarine sulcus occurs first (together with P1 generators), at a latency of 87 ms. According to previous work (Martinez et al., 2001; Di Russo et al., 2003), this fMRI activation corresponds to the C1 peak from the POz electrode, and appears at a latency of 50-60 ms. This peak, however, cannot be captured with the PO7 and PO8 electrodes, resulting in ERP amplitude values close to zero at t=50-60 ms in our data. Consequently, the $fMRI_{movie}$ variable can have no activation at that time instant (see equation (2)). Nonetheless, this area is apparently successfully associated to the first fMRI activation.

Concerning the P1 and N1 generators, they are present at latencies and spatial coordinates which are very close to the ones presented in Di Russo et al. (2003). These spatial coordinates are shown explicitly in Table 1. This finding is even more significant taking into account that in Di Russo et al. (2003), the generators are obtained by dipole modeling of the ERPs, and then back-projected to the fMRI map, whereas in our study, they are obtained in fully data-driven way, i.e. using the JointICA decomposition.

Additional analyses: Central linking hypothesis

To understand the performance of the JointICA more fully and to be able to explain how and why it works, we performed several additional analyses as described in the Methods section. To begin with, we tested what is the influence of the ICA algorithm used in

JointICA. All the results so far have been obtained with the Infomax algorithm (Bell and Sejnowski, 1995). We also applied here another well-known ICA algorithm JADE (Cardoso and Souloumiac, 1993), which maximizes the statistical independence of the components by diagonalizing the 4th order cumulant of the mixing matrix. The results are not presented here in detail, but they show several disadvantages when compared to the Infomax results. First, the independent component revealing the N1 peak in the ERP modality did not show any interpretable fMRI activation. Second, the motor component of the fMRI modality was not connected to any of the ERP independent components. Furthermore, the P1- and P2-related components were connected to bilateral visual field activations, which is in conflict with earlier findings in literature.

Also we compared the ERP and fMRI decompositions obtained by JointICA analysis, to those obtained by applying Infomax to solely fMRI or outside recorded ERP data. The result of the Infomax decomposition of the ERP data corresponding to the down left stimulus is shown in Fig. 6.

It is clear that the P2 peak is separated in two different components (magenta and light-blue), whereas this was not the case when JointICA was applied (Fig. 2). This might be because the magenta component describes the P2 latency difference over subjects and has no strong interpretation in the fMRI modality. However, we checked the distribution of this component over subjects, and we are not able to strongly support this argument. Nevertheless, we use this as a proof that not only the JointICA fMRI decomposition is influenced by the ERP modality, but that vice versa also holds. Other components are very similar to the ones obtained by JointICA and therefore seem less dependent on the fMRI information.

The Infomax source separation of the fMRI modality is not presented here, but in Table 2 we provide the correlations between the results from ICA performed only on EEG and the JointICA EEG results (first row) and between the results from ICA on fMRI and the JointICA fMRI results (second row). For each case, also the mean per category is provided. Statistical significance has been checked with the student paired t-test and a *p*-value was computed ($p<0.05$).

From this table it is obvious that the correlations between the results from the ERP decomposition performed solely, and the ones from the joint analysis, are much higher than it is the case for the fMRI maps for category 1 components. This means that the ERP part of the JointICA components changes much less than the fMRI part, relative to single modal ICA decompositions (performed solely on ERP or fMRI data). This is an indication that the ERP modality is the one driving the joint decomposition, and improves the decomposition of the fMRI data. On the other hand, as already mentioned above, the P2 peak from Fig. 6 is separated in two independent components, whereas it belongs to only one IC when the joint analysis is performed (Fig 3.). That means that fMRI also influences the decomposition of the ERP, so that the joint analysis is not completely one-sided either. However, the influence of the ERP seems to be stronger, implying that high quality ERPs are of major importance.

As a reference, we also checked the spatial similarity between fMRI maps derived with ERP data recorded inside and outside the scanner room. The spatial correlation coefficients are shown in the upper row of Table 3, and indicate that inside recorded ERP significantly improves the fMRI decomposition, compared to the separation when no ERP is used (bottom row of Table 2), especially for the components from the first category (mean values are 0.65 for the inside ERP, compared to 0.46 when no ERP data

are used for decomposition). For the other two categories, the difference is barely visible. The conclusion for the category 1 independent components is consistent with the visual observation of Fig. 3.

To further investigate the importance of the central linking hypothesis, the lower row of Table 3 shows the correlation coefficients between the fMRI IC maps derived in a regular way with outside recorded ERPs and the fMRI IC maps derived with outside ERP data randomly assigned to the fMRI maps (i.e. the fMRI and the ERP data of the subjects do not correspond to each other). It is clear that the independent components from category 1 and 2 yield very low correlations with the randomized data. Moreover, these correlations are much worse compared to the decomposition when inside recorded ERPs were used. On the other hand, the category 1 components show similarly low correlations when data are randomized and when the data are decomposed without ERPs (lower row of Table 2). Additionally, when the data are randomized, the fMRI maps are connected to the wrong EEG peak components, similarly as when JADE was applied. This leads to the conclusion that the decomposition with randomized ERPs is as bad as when no ERP information is used. However, since the ERP data are present, and therefore still influence the decomposition, the individual correlations differ between particular fMRI independent maps for randomized data and when no ERP data were used, although on average the values do not differ significantly.

Additional analyses: Robustness

The robustness of the JointICA results is evaluated in Table 4, showing the correlation between the fMRI spatial maps of the independent components extracted with all 15 subjects, and the maps from the cases where we omit 2, 3, 4 and 5 subjects, respectively.

From this robustness analysis, we can conclude that IC number 6, which corresponds to the N1 peak (Fig. 3), is consistently present for any number of subjects. This is visible since the correlation coefficients for this component, given in column 6 of Table 4, are very high (above 0.9). It is interesting to note that there are also other very robust fMRI ICs (e.g. 2, 3, 4, and 8), which are mostly from category 3 (having no ERP interpretation).

On the other hand, correlation coefficients for ICs 1 and 9 from Fig. 6 are dropping rather fast, when the number of subjects participating in the study is below 13. This indicates that the number of subjects used for JointICA should not be too low. This is expected, since it is assumed by the ICA algorithm that the number of sources is smaller than the number of recordings (subjects). When we estimate fewer sources than present in the data, the algorithm starts to be strongly inaccurate. Also, the data dimension is very large, which probably leads to the higher number of real sources than 12, what is used in our analyses.

Discussion

In this study we evaluated and presented the performance of JointICA, a recently proposed method for a symmetric integration of EEG and fMRI. To this end, we recorded EEG and fMRI data during a simple visual detection task. We compared the performance of JointICA for data acquired both simultaneously and non-simultaneously and

investigated whether the decomposition was equally driven by both modalities, or solely by one of them. Moreover, we examined the validity and necessity of the assumptions that JointICA relies on (Calhoun et al., 2006), the importance of the amount of available data and the selection of the ICA algorithm. Performing JointICA on EEG and fMRI data measured simultaneously resulted in meaningful components. Making use of EEG data measured outside of the scanner room, however, clearly improved the interpretability of the results and yielded spatio-temporal activations more consistent with the literature (Di Russo et al., 2003). In addition, the obtained JointICA ERP ICs were very similar to the ones retrieved with ICA performed on the ERPs alone.

According to the literature and based on the characteristics of the presented task, the P1 and N1 peaks found in the ERPs are expected to correspond to extrastriate visual activations in fMRI (Di Russo et al., 2003). In addition, our subjects were required to respond to the presented stimuli by pressing a button, which should evoke activation of the motor-related cortex occurring concurrently with the N1 wave (Calhoun et al., 2006). The results obtained with the JointICA analysis both on simultaneously and non-simultaneously acquired data confirm these expectations to a certain extent, hereby validating the performance of this method as shown previously (Calhoun et al., 2006, 2009, 2010; Franco et al., 2008; Xu et al., 2009).

However, in the simultaneous results the motor activation did not correspond to any of the ERP components, whereas there was a clear N1 correspondence in the non-simultaneous measurements. As this difference is probably connected to residual EEG artifacts, acquiring EEG and fMRI data in separate sessions might be a good procedure in certain circumstances. However, if one would opt for single-trial ERP-fMRI analyses (e.g. with JointICA like in Moosmann et al., 2008) simultaneous recordings are definitely

to be preferred. Moreover, there are many cognitive studies in which processes, such as habituation and arousal state (Debener et al., 2005, 2006), play an important role, and thus simultaneous measurements have to be performed. In both cases, it is essential to carefully optimize the data quality (e.g., Vanderperren et al., 2010) prior to further analyses.

In this context, our results also show that increasing the number of subjects has a clear impact on the quality of the decomposition. As such, including more subjects in the analysis might further facilitate obtaining sufficient data quality, especially in the case of the simultaneous recordings.

To find an answer to the question about which modality is driving the JointICA decomposition, we performed a correlation analysis to compare similarity of components obtained from integrated and individual ERP and fMRI ICA analyses. Since the correlation values were significantly higher for the ERP compared to the fMRI modality, we hypothesize that the JointICA decomposition is more strongly driven by the ERP characteristics. Not only is this finding important to understand the principles behind the JointICA method, but it also represents an additional argument for optimizing the quality of the ERP data.

However, the decomposition is not completely asymmetric either, since including fMRI also influences the ERP component separation. This is especially apparent if we compare Figs. 3 and 6, and pay attention to the P2 peak. This peak is separated in two different components when ICA is applied to only ERP data, whereas they were extracted together in a single component in the case of JointICA.

Even though we know now which data properties are important to retrieve interpretable ICA components, this does not yet explain why exactly the JointICA

method is able to extract these specific multimodal components. If you would consider general ICA assumptions, obtaining these components does not seem logical for the following reasons. First of all, the fMRI activation maps in the brain have no physiological ground to be statistically independent from each other. This is why algorithms based on e.g. the diagonalization of 4th order cumulant matrices (like JADE), are not able to separate fMRI sources (Calhoun et al., 2001; Corea et al., 2007). Second, there is no reason to assume that ERP temporal peak components and fMRI spatial independent maps are statistically dependent, and will therefore be extracted into one independent component.

As described in Calhoun et al. (2006), however, JointICA makes use of the Infomax algorithm. The superior performance of this algorithm, compared to other algorithms, for fMRI applications has been shown by different groups (McKeown et al., 1998b; Calhoun et al., 2001,2003; Daubechies et al., 2009). It was proven by Daubechies et al. (2009) that the performance of Infomax is linked to its ability to effectively handle sparse components rather than independent components as such. An explanation for this can be found in the fact that Infomax is based on an information-maximization criterion, which does not strictly imply statistical independence between components. For this reason, we expect Infomax not only to perform well on the fMRI but also on the joint data, since it will automatically connect signal parts that behave similarly. For a more theoretical explanation, we refer the reader to Daubechies et al. (2009).

This means that, for Infomax to work, brain areas corresponding to higher ERP peak amplitudes also need to show stronger hemodynamic responses and vice versa. If the amplitude modulation over subjects is the same and linearly dependent between both

modalities, due to equation (1) they will be captured in the same row of the **S** matrix, i.e. in the same independent component.

To support our hypothesis that the activations in ERP and fMRI data are indeed highly correlated, we refer to work of Sadeh et al. (2010) for visual brain activation in humans. In this study, they examined the correlations between ERP and fMRI measures in face-selectivity. What they found is that not only face-selective ERP and fMRI responses were highly-correlated, but also that these correlations were specific for distinct ERP latencies and distinct brain regions. Following the same logic, we believe that these findings hold for all brain activations and that different ERP peak components are highly connected to different fMRI regions. This was also confirmed in a similar study with auditory stimulation by Mayhew et al. (2010).

However, contrary to what is assumed in literature (Calhoun et al., 2006; Corea et al., 2010) the amplitude modulations do not have to change in exactly the same way. If the modulations are not exactly the same but similar, Infomax will generate one component capturing the similarity between components, and another one containing the difference. These components will be connected to differences between individual ERP responses.

Conclusion

In this study we investigated the performance of JointICA for EEG-fMRI data on a visual detection task. We showed and compared the performance when the EEG was recorded both simultaneously with fMRI data and in a separate session (outside the scanner room).

We showed that the joint decomposition is mostly driven by the ERP modality, and that therefore a good quality of the ERP data is highly desirable. It is also shown that the number of subject participants should be as high as possible, in order to obtain a meaningful decomposition. The importance of the ICA algorithm, which is used for the decomposition, is also analyzed and discussed. Although it was shown previously that infomax is the best suited algorithm for this application, it was closer explained in the discussion section of this manuscript why exactly this algorithm is the best choice.

Acknowledgements

Research supported by

- Research Council KUL: GOA Ambiorics, GOA MaNet, CoE EF/05/006 Optimization in Engineering (OPTEC), PFV/10/002 (OPTEC), IDO 05/010 EEG-fMRI, IDO 08/013 Autism, IOF-KP06/11 FunCopt, several PhD/postdoc & fellow grants;
- Flemish Government:
    - FWO: PhD/postdoc grants, projects: FWO G.0302.07 (SVM), G.0341.07 (Data fusion), G.0427.10N (Integrated EEG-fMRI) research communities (ICCoS, ANMMM);

  - IWT: TBM070713-Accelero, TBM070706-IOTA3, TBM080658-MRI (EEG-fMRI), PhD Grants;
  - IBBT
- Belgian Federal Science Policy Office: IUAP P6/04 (DYSCO, `Dynamical systems, control and optimization', 2007-2011);ESA PRODEX No 90348 (sleep homeostasis)
- EU: FAST (FP6-MC-RTN-035801), Neuromath (COST-BM0601)

JW is supported by long-term structural funding from the Flemish Government (METH/08/02).

The scientific responsibility is assumed by its authors.

References

Allen P. J., Josephs O., and Turner R., 2000. *A method for removing imaging artifact from continuous EEG recorded during functional MRI*. NeuroImage 12, 230-239.

Bell A.J., and Sejnowski T.J., 1995. *An Information-Maximisation Approach to Blind Separation and Blind Deconvolution.* Neural Comput. 7 (6), 1129-1159

Bénar, C.G., Grova, C., Kobayashi, E., Bagshaw, A.P., Aghakhani, Y., Dubeau, F., Gotman, J., 2006. *EEG–fMRI of epileptic spikes: Concordance with EEG source localization and intracranial EEG*. NeruoImage 30 (4), 1161-1170.

Calhoun V.D., Adali T., Pearlson G.D, and Pekar J.J., 2001. *A Method for Making Group Inferences from Functional MRI Data Using Independent Component Analysis.* Hum. Brain Mapp. 14, 140-151

Calhoun V.D., Adali T., Hansen L.K., Larsen J., Pekar J.J. 2003 *ICA of Functional fMRI data: An Overview.* In Proc. Int. Workshop on ICA and BSS, 281-288

Calhoun V.D., and Pearlson G.D., 2004. *Independent Components Analysis Applied to FMRI Data: A Generative Model for Validating Results*. J. VLSI Signal Proc. 37, 281-291

Calhoun V.D., Adali T., Pearlson G.D., and Kiehl K.A., 2006. *Neuronal chronometry of target detection: Fusion of hemodynamic and event-related potential data*. NeuroImage 30, 544-553.

Calhoun V.D., Liu J., Adali T., 2009. *A review of group ICA for fMRI data and ICA for joint inference of imaging, genetic, and ERP data*. NeuroImage 45(1 Suppl), 163-172

Calhoun V.D., Wu L., Kiehl K.A., Eichele T., Pearlson G.D., 2010. *Aberrant processing of deviant stimuli in schizophrenia revealed by fusion of fMRI and EEG data.* Acta Neurpsychiatr. 22(3), 127-138

Cardoso J.F., Souloumiac A., 1993. *Blind beamforming for non-Gaussian signals.* IEE Proc.-F 140 (3), 362-370

Corea N.M., Li Y.O., Adali T., and Calhoun V.D., 2008. *Canonical Correlation Analysis for Feature-Based Fusion of Biomedical Imaging Modalities and Its Application to Detection of Associative Networks in Schizophrenia*. IEEE J. Sel. Top. Signa. 2 (6), 998-1007

Corea N., Adali T., and Calhoun V.D., 2007. *Performance of Blind Source Separation Algorithms for fMRI using a Group ICA Method.* Magn. Reson. Imaging 25, 684-694

Corea N., Li Y.O., Adali T., and Calhoun V.D., 2010. *Canonical Correlation Analysis for Data Fusion and Group Inference*. IEEE Signal Proc. Mag. 39, 39-50

Czisch, M., Wetter, T.C., Kaufmann, C., Pollmacher, T., Holsboer, F., Auer, D.P., 2002. *Altered processing of acoustic stimuli during sleep: reduced auditory activation and visual deactivation detected by a combined fMRI/EEG study*. NeuroImage 16, 251–258.

Daubechies I., Roussos E., Takerkart S., Benharrosh S., Golden C., D'Ardenne K., Richter W., Cohen J.D., and Haxby J., 2009. *Independent component analysis for brain fMRI does not select for independence.* P. Natl. Acad. Sci. USA. 106(26), 10415-10422

De Vos M., Ries S., Vanderperren K., Vanrumste B.. Alario F-X., Van Huffel S. and Burle B., 2010. *Removal of muscle artifacts from EEG recordings of spoken language production.* Neuroinformatics 8(2), 135-150.

De Vos M., Vergult A., De Lathauwer L., De Clercq W., Van Huffel S., Dupont P., Palmini A., Van Paesschen W., 2007. *Canonical decomposition of ictal scalp EEG reliably detects the seizure onset zone.* NeuroImage 37(3), 844-854.

Debener, S., Ullsperger, M., Siegel, M., Fiehler, K., von Cramon, D.Y., Engel, A.K., 2005. *Trial-by-trial coupling of concurrent electroencephalogram and functional magnetic resonance imaging identifies the dynamics of performance monitoring*. J. Neurosci. 25 (50), 11730–11737.

Debener, S., Ullsperger, M., Siegel, M., Engel, A.K., 2006. *Single-trial EEG–fMRI reveals the dynamics of cognitive function*. Trends Cogn. Sci. 10 (12), 558–563.

Debener S., De Vos M., 2011. *The benefits of simultaneous EEG-fMRI for EEG analysis.* Clin. Neurophysiol. 122 (2), 267-277.

Delorme A., and Makeig S., 2004. *EEGLAB: an open source toolbox for analysis of single-trial EEG dynamics including independent component analysis*. J Neurosci. Meth. 134, 9-21.

Di Russo F., Martinez A., Hillyard S.A., 2003. *Source analysis of event-related cortical activity during visuo-spatial attention*. Cereb. Cortex 13, 486-499.

Di Russo F., Pitzalis S., Spitoni G., Aprile T., Patria F., Spinelli D., Hillyard S.A., 2005. *Identification of the neural sources of the pattern-reversal VEP*. NeuroImage 24, 874-886.

Eichele, T., Calhoun, V.D., Moosmann, M., Specht, K., Jongsmae, M.L.A., Quian Quiroga, R., Nordby, H., Hugdahl, K., 2008. *Unmixing concurrent EEG-fMRI with parallel independent component analysis.* Int. J. Psychophysiol. 67 (3), 222–234.

Franco A.R., Ling J., Caprihan A., Calhoun V.D., Jung R.E., Heileman, G.L., Mayer A.R., 2008. *Multimodal and Multi-Tissue Measures of Connectivity Revealed by Joint Independent Component Analysis*. IEEE J. Sel. Top. Signa. 2 (6), 986-997

Goldman, R.I., Stern, J.M., Engel, J.Jr., and Cohen, M.S., 2000. *Acquiring simultaneous EEG and functional MRI*. J. Clin. Neurophysiol. 111, 1974–1980.

Goldman, R.I., Stern, J.M., Engel, J.Jr., and Cohen, M.S., 2002, *Simultaneous EEG and FMRI of the alpha rhythm.* NeuroReport 13, 2487–2492.

Kim K.H., Yoon H.W., Park H.W., 2004. *Improved ballistocardiac artifact removal from the electroencephalogram recorded in fMRI.* J. Neurosci. Meth. 135 (1–2), 193–203.

Krakow, K., Lemieux, L., Messina, D., Scott, C.A., Symms, M.R., Duncan, J.S., Fish, D.R., 2001. *Spatio temporal imaging of focal interictal epileptiform activity using EEG-triggered functional MRI*. Epileptic Disord. 3 (2), 67-74

Laufs, H., Kleinschmidt, A., Beyerle, A., Eger, E., Salek-Haddadi, A., Preibisch, C., Krakow, K., 2003. *EEG-correlated fMRI of human alpha activity*. NeuroImage 19, 1463–1476.

Lemieux, L., Salek-Haddadi, A., Josephs, O., Allen, P., Toms, N., Scott, C., Krakow, K., Turner, R., Fish D.R., 2001. *Event-Related fMRI with Simultaneous and Continuous EEG: Description of the Method and Initial Case Report*. NeuroImage 14 (3), 780-787.

Liebenthal, E., Ellingson, M.L., Spanaki, M.V., Prieto, T.E., Ropella, K.M., Binder, J.R., 2003. *Simultaneous ERP and fMRI of the auditory cortex in a passive oddball paradigm*. NeuroImage 19, 1395–1404.

Logothetis, N.K., Pauls, J., Augath, M., Trinath, T., Oeltermann, A., 2001. Neurophysiological investigation of the basis of the fMRI signal. Nature 412, 150-157.

Martinez A., DiRusso F., Anllo-Vento L., Sereno M.I., Buxton B.B., Hillyard S.A., 2001. *Putting spatioal attention on the map: timing and localization of stimulus selection process in striate and extrastriate visual areas.* Vision Res. 41, 1437-1457

Mayhew S.D., Dirckx S.G., Niazy R.K., Iannetti G.D., and Wise R.G**.,** 2010. *EEG signatures of auditory activity correlate with simultaneously recorded fMRI responses in humans*. NeuroImage 49(1), 849-864

McKeown M.J., and Sejnowski T.J., 1998a. *Independent Component Analysis of fMRI Data: Examining the Assumptions.* Hum. Brain Mapp. 6, 368-372.

McKeown M.J., and Sejnowski T.J., Makeig A., Brown G.G., Jung T.P., Kindermann S.S., Bell A.J., and Sejnowski T.J., 1998b. *Analysis of fMRI Data by Blind Separation Into Independent Spatial Components.* Hum. Brain Mapp. 6, 160-188.

McKeown M.J., 2000. *Detection of Consistently Task-Related Activations in fMRI Data with Hybrid Independent Component Analysis*. NeuroImage 11, 24-35

Moosmann, M., Ritter, P., Krastel, I., Brink, A., Thees, S., Blankenburg, F., Taskin, B., Obrig, H., Villringer, A., 2003. *Correlates of alpha rhythm in functional magnetic resonance imaging and near infrared spectroscopy*. NeuroImage 20, 145–158.

Moosmann, M., Eichele, T., Nordby, H., Hugdahl, K., Calhoun, V.D., 2008. *Joint independent component analysis for simultaneous EEG-fMRI: principle and simulation.* Int. J. Psychophysiol. 67 (3), 212–221.

Moosmann M., Schonfelder V. H., Specht K., Scheeringa R., Nordby H., and Hugdahl K., 2009. *Realignment parameter-informed artefact correction for simultaneous EEG-fMRI recordings.* NeuroImage 45, 1144-1150.

Mulert, C., Jäger, L., Schmitt, R., Bussfeld, P., Pogarell, O., Möller, H.J., Juckel, G., Hegerla, U., 2004. *Integration of fMRI and simultaneous EEG: towards a comprehensive understanding of localization and time-course of brain activity in target detection*. NeuroImage 22, 83–94.

Mulert C., Lemieux L., 2010. *EEG-fMRI: Psychological Basis, Technique and Applications.* Springer.

Niazy R. K., Beckmann C. F., Iannetti G. D., Brady J. M., and Smith S. M., 2005. *Removal of FMRI environment artifacts from EEG data using optimal basis sets.* NeuroImage 28, 720-737.

Novitskiy N., Ramautar J.R., Vanderperren K., De Vos M., Mennes M., Mijovic B., Vanrumste B., Stiers P., Van den Bergh B., Lagae L., Sunaert S., Van Huffel S., Wagemans J., 2011. *The BOLD correlates of the visual P1 and N1 in single-trial analysis of simultaneous EEG-fMRI recordings during a spatial detection task.* NeuroImage, 54(2), 824-835

Roy C. S., and Sherrington C. S. *On the Regulation of the Blood-Supply of the Brain*., 1890. Journal of Physiology, 85-108

Sadeh B., Podlipsky I., Zhdanov A., and Yovel1 G., 2010. *Event-Related Potential and Functional MRI Measures of Face-Selectivity are Highly Correlated:A Simultaneous ERP-fMRI Investigation*. Hum. Brain Mapp. 31 (10) 1490-1501.

Schabus, M., Dang-Vu, T.T., Albouy, G., Balteau, E., Boly, M., Carrier, J., Darsaud, A., Degueldre, C., Desseilles, M., Gais, S., Phillips, C., Rauchs, G., Schnakers, C., Sterpenich, V., Vandewalle, G., Luxen, A., Maquet, P., 2007. *Hemodynamic cerebral correlates of sleep spindles during human non-rapid eye movement sleep*. Proc. Natl. Acad. Sci. USA. 104, 13164–13169.

Seeck, M., Lazeyras, F., Michel, C.M., Blanke, O., Gericke, C.A., Ives, J., Delavelle, J., Golay, X., Haenggeli, C.A., de Tribolet, N., Landis, T., 1998. *Non-invasive epileptic focus localization using EEG-triggered functional MRI and electromagnetic tomography*. Electroen. Clin. Neur. 106 (6), 508-512.

Ullsperger M., Debener S., 2010. *Simultaneous EEG and fMRI, Recording, Analysis and Application*. Oxford University Press (New York).

Vanderperren K., De Vos M., Ramautar J.R., Novitskiy N., Mennes M., Assecondi S., Vanrumste B., Stiers P., Van den Bergh B.R.H., Wagemans J., Lagae L., Sunaert S., Van Huffel S., 2010. *Removal of BCG artifacts from EEG recordings inside the MR scanner: a comparison of methodological and validation-related aspects*. NeuroImage 50(3), 920-934.

Viola F.C., Thorne J., Edmonds B., Schneider T., Eichele T., Debener S., 2009. *Semi-automatic identification of independent components representing EEG artifact.* Clin. Neurophysiol. 120 (5), 868-877

Xu L., Pearlson G., Calhoun V.D., 2009. *Joint source based morphometry identifies linked gray and white matter group differences*. NeuroImage 44(3), 777-789

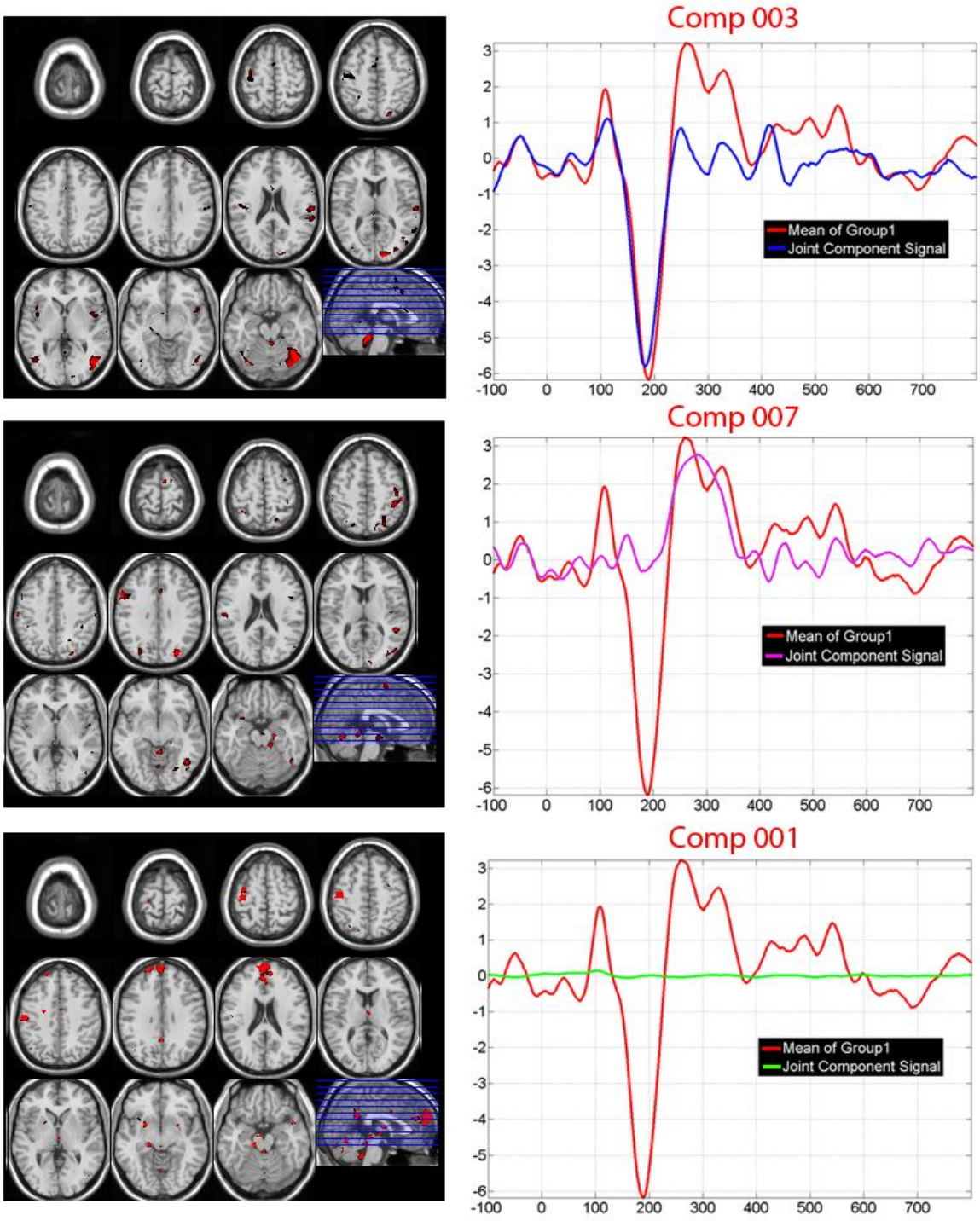

Figure 1. The results of JointICA for the data recorded with the down-left stimuli. Every extracted source contains an fMRI and an ERP part. The fMRI activations are shown on axial sections on the left (the bottom right corner shows the axial sections that are represented in the figure). The blue, green or magenta curve on the right visualizes the ERPs. In addition, the grand average ERP is

included in the right column in red. We see that the first component (top row – Comp 003) captures the P1 and N1 components together, with spatial activations unilateral in the upper flank of right calcarine sulcus (BA17; 14,-94,14), representing the early visual areas activation, and bilateral but with right-ward assymetry, in middle occipital gyrus (BA19; 46,-72,6), and the posterior fusiform gyrus (BA19; 40,-66,-18), corresponding to activations in extrastriate visual areas. The second component (middle row - Comp 007) captures the P2 ERP component, and spatially activates the right anterior intraparietal sulcus (BA7; 26,-64,56), the right posterior intraparietal sulcus (BA19; 28,-78,30) and the right postcentral sulcus (BA2, 44,-36,56). The third component (bottom row – Comp 001) is not connected to any ERP activation. This fMRI component shows activity in the left postcentral gyrus (BA3; -48,-16,54) - which corresponds to primary somatosensory cortex, and the anterior medial prefrontal cortex (BA10; 2,66,26).

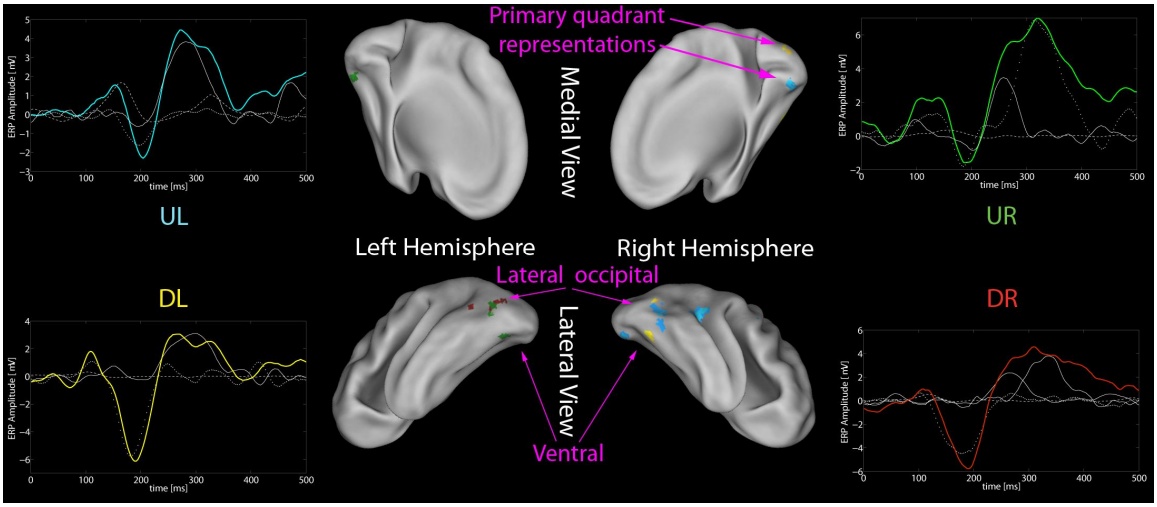

Figure 2. The first brain activations that occur in the ERP-fMRI movie for the simultaneously recorded data. The offset is around 90-100 ms, depending on the presented stimuli. The grand average ERPs (in color), and the ERP ICs (white) of the particular stimuli are shown in the corners of the figure, such that their position describes the corresponding stimulus (i.e. the ERP corresponding to the upper left stimulus is presented in the upper left corner of the figures, and the down left, down right and upper right stimuli are presented in the counter clockwise order). The ERP independent components (in white), are presented such that dashed, dotted and solid line correspond to P1, N1, and P2 ERP waves respectively. In the middle of the figure, the functional activations are plotted on the inflated brain. Left and right hemispheres are presented on the left-

and right-hand side respectively. The medial view above, and the lateral view is given below the imaginary horizontal central line of the figure. Each functional activation is painted in the same color as the corresponding grand-average ERP for the sake of clarity.

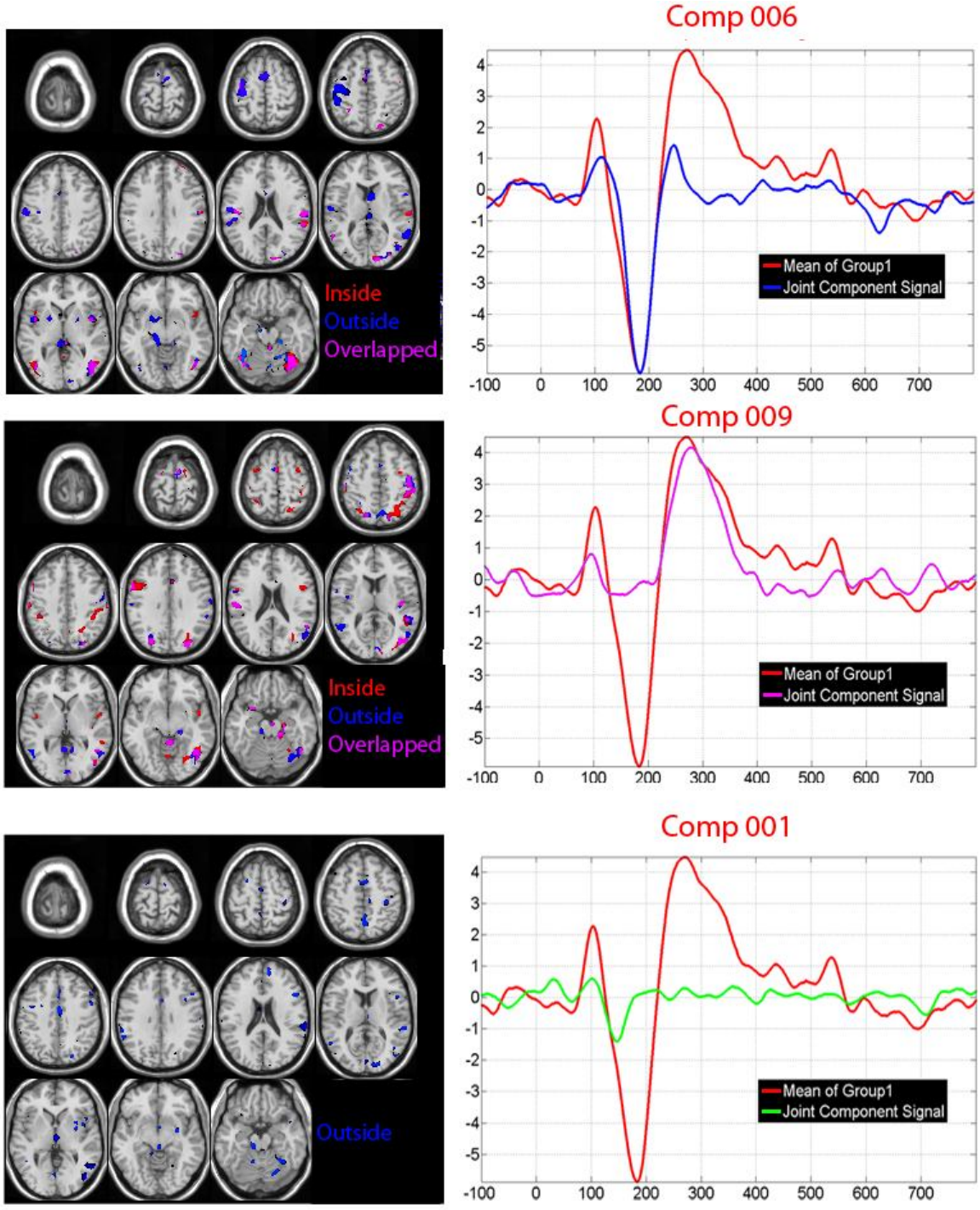

Figure 3. The fMRI activations in blue (left) and their related ERP components in blue, green or magenta color (right) obtained by JointICA for the non-simultanously recorded data. In addition, the fMRI data from the simultanously recorded measurements are presented in red, and the overlap between simultanous and non-simultanous measurements is shown in magenta. The grand average ERP is shown in red in the right column. The first component (top row – Comp 6) captures the P1 and N1 components together, with spatial activations in both right and left middle occipital gyrus (BA19; 44,-74,6 - LOC area), area with coordinates (40,-66,-18), primary visual cortex (BA17; 14,-94,14 – V1/V2 area). It also shows activation in the left postcentral gyrus (BA3; -48,-16,54) – corresponding to the primary somatosensory cortex, and superior frontal gyrus (BA10; 2,66,26). The second component (middle row - Comp 009 captures the P2 ERP component, and spatially activates the right parietal precuneus (BA7; 26,-64,56), right inferior parietal lobule (BA40; 44,-36,56), right occipital precuneus (BA31; 28,-78,30). The third component (Comp 001) shows no interpretable fMRI activation. It is a consequence of different latencies of the N1 peak in different subjects.

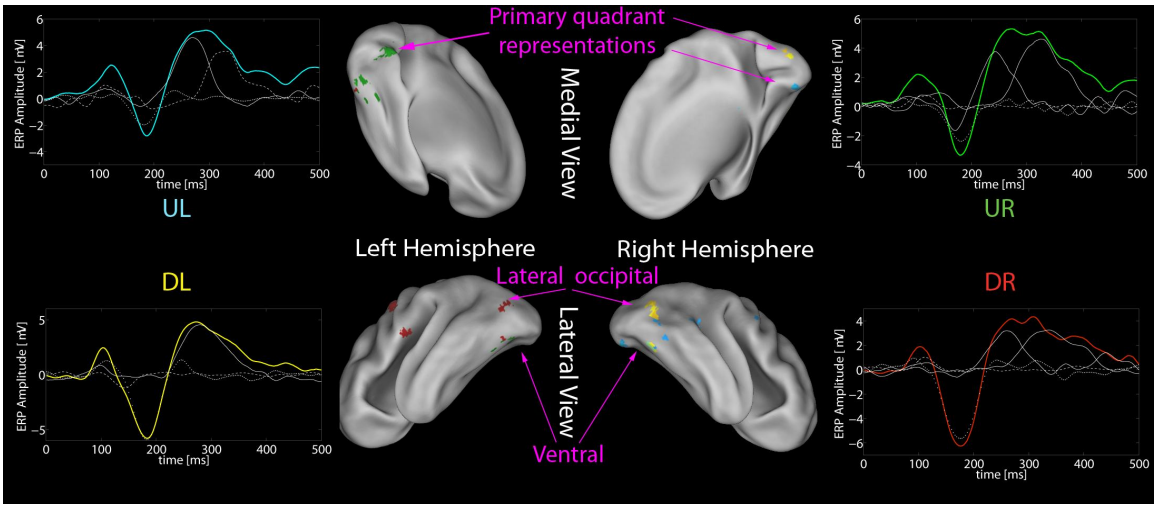

Figure 4. Analogue to Fig. 2 the first brain activations that occur in the ERP-fMRI movie for the non-simultaneously recorded data are shown. The offset is around 90-100 ms, depending on the presented stimuli. The grand average ERPs (in color), and the ERP ICs (white) of the particular stimuli are shown in the corners of the figure, such that their position describes the corresponding stimulus (i.e. the ERP corresponding to the upper left stimulus is presented in the upper left corner of the figures, and the down left, down right and upper right stimuli are presented in the counter

clockwise order). The ERP independent components (in white), are presented such that dashed, dotted and solid line correspond to P1, N1, and P2 ERP waves respectively. In the middle of the figure, the functional activations are plotted on the inflated brain. Left and right hemispheres are presented on the left- and right-hand side respectively. The medial view above, and the lateral view is given below the imaginary horizontal central line of the figure. Each functional activation is painted in the same color as the corresponding grand average ERP for the sake of clarity.

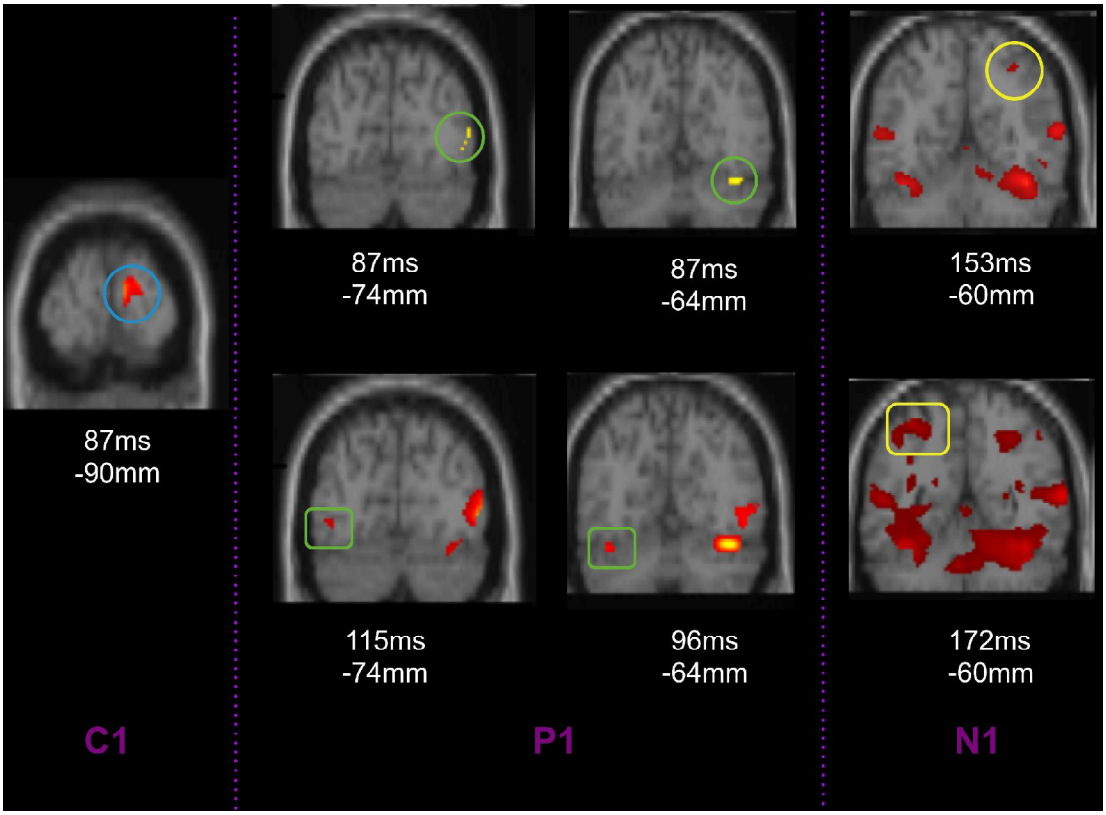

Figure 5. Visual fMRI activations (C1, P1, and N1) in order of appearance (from left to right). Circles denote the contra-lateral activations of a particular component, and rectangles show their corresponding mirror activations on the ipsi-lateral side. Millimeter values are Talaraich *Y* coordinates of the slices that include fMRI activations. The complete Talaraich coordinates are provided in Table 1. Under each fMRI slice, the time at which the particular activation appears for the first time, is denoted.

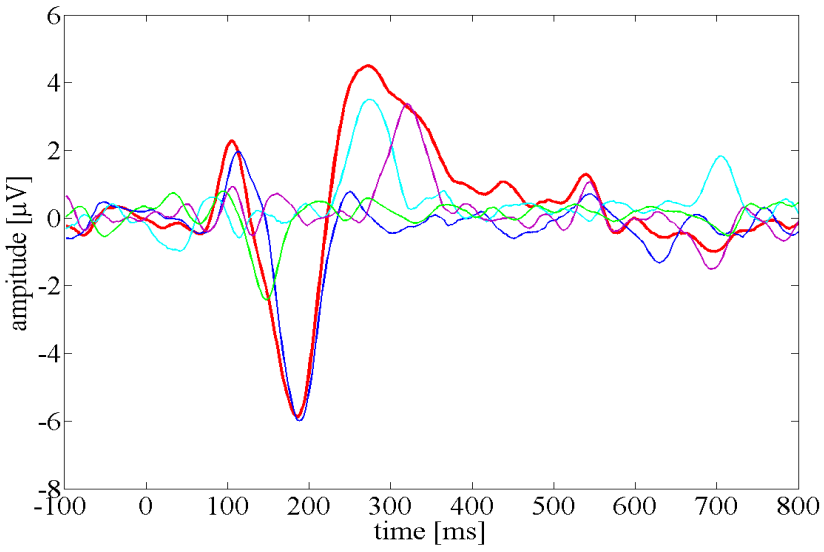

Figure 6 The Infomax extraction of the independent components from the ERP data. The data correspond to down-left stimuli from the outside dataset. The grand-average ERP is shown in red. Other colors show different wave components. Only the 4 peak-related components (out of 12 extracted) are shown (this corresponds to category 1 ICs in the joint analysis).